(dual-frequency)-dependent dynamic functional connectivity analysis of visual working memory capacity

John Aston, Dominique Dehay, Anna E. Dudek, Jean-Marc Freyermuth, Denes Szucs, Lincoln Colling

(dual-frequency)-dependent dynamic functional connectivity analysis of visual working memory capacity

John Aston
Department of Pure Mathematics and Mathematical Statistics,
University of Cambridge, U.K.
and
Dominique Dehay
Univ Rennes, CNRS, IRMAR UMR 6625, France
and
Anna Dudek
AGH University of Science and Technology, Dept. of Applied Mathematics, Poland *
and
Jean-Marc Freyermuth
Institut de Mathématiques de Marseille, Aix-Marseille University, France.
and
Denes Scuzs
Department of Psychology, University of Cambridge, U.K.†
and
Lincoln Colling
Department of Psychology, University of Cambridge, U.K.

May 18, 2019

Abstract

In this paper we develop a novel methodology for studying the dynamic functional connectivity within the brain from EEG traces. Our observations consist of replicated realizations of spatio-temporal processes that are locally time-harmonizable. We propose a novel method to estimate both the spatial time-varying Loève-spectrum and the spatial time-varying dual-frequency coherence functions under realistic modeling assumptions. We apply block bootstrap approach to construct confidence intervals for these parameters of interest. We illustrate the application of this methodology on a data set arising from an experiment designed to assess the visual working memory capacity. Our real data analysis pipeline starts with the clustering of our replicated time series obtained from toroidal mixture modeling of the corresponding response variables which describe the quality of memorization. Then, we estimate the spatial time-varying dual-frequency coherence functions and the corresponding connectivity matrices within each cluster. This procedure allows us to potentially identify specific patterns in the dynamic functional connectivity characterizing each cluster. More specifically we reveal that better visual working memory performance is apparently associated to longer connectivity period within the prefrontal cortex between the alpha-beta frequency bands during the memorization task.

Keywords: Harmonizable spatio-temporal processes, functional connectivity, visual working memory, EEG traces, Circular Block Bootstrap.

*Anna Dudek was partially supported by the Faculty of Applied Mathematics AGH UST statutory tasks within subsidy of Ministry of Science and Higher Education.

†Denes Scuzs and Lincoln Colling are funded by James S. McDonnell Foundation 21st Century Science Initiative in Understanding Human Cognition (grant number 220020370; received by Denes Scuzs).

1 Introduction

Working Memory (WM) is an essential cognitive resource since it is strongly correlated to the overall cognitive abilities. Its role is to keep relevant information accessible during a brief time-span which enables for human activity alike navigation, communication, solving problems... The study of the brain mechanisms underlying WM often rely on ElectroEncephaloGraphy (EEG) techniques. In short, the electrical currents generated in the brain by ensembles of neurons which fires in a synchronized manner propagate through the cortex to the scalp where they are recorded by EEG electrodes. These electrodes measure electric potentials over the time which represents brain waves oscillations. Spectral analysis is a key tool for neuroscientists for inference on these time series data. Previous studies have shown variations in the dynamic of different frequency bands associated to WM tasks but the role of each of them remains unclear.

Over the last 20 years there has been an explosion of more specific research on Visual Working Memory (WSM). We define VWM following Luck and Vogel (2013) as an "active maintenance of visual information to serve the needs of ongoing tasks". There are key issues at stake in describing and identifying the sources of limitation and variability of the VWM (Fougnie et al., 2012). VWM presumably involves sophisticated functional connections within different areas of the brain, in particular the visual cortex and the prefrontal cortex appears to play fundamental roles (Grimault et al., 2009; Li et al., 2011; Barton and Brewer, 2013; Dai et al., 2017). Elucidating the nature of these connections is supposedly a doorway to fruitful inference on these brain cognitive processes. There are different ways to assess the existence of these connections. The coherence, which is a spectral cross-correlation between two signals, has proved to be useful to reveal interesting facts for WM (Sauseng et al., 2005). A challenging aspect is that these dynamic functional connections may involve

brain waves' oscillatory components of possibly different frequencies (Gorrostieta et al., 2012; Pascual-Marqui et al., 2016). In other terms, bursts of high frequencies in some area of the brain could occur preferentially during specific phases of low frequency activity in other areas.

It is therefore essential to develop methods to accurately estimate the dynamics of the coherence between different part of the brain at different oscillating frequencies, so-called dual-frequency coherence hereafter. The use of the dual-frequency coherence in EEG data analysis is not new (Gündoğdu and Akan (2010); Gorrostieta et al. (2019)). From a mathematical perspective, in order to model the dual-frequency coherence, we require a proper class of stochastic processes named harmonizable which naturally generalize the class of stationary processes (see Section 2). They were introduced in the stochastic analysis literature by Loève (1948) and are associated to a generalized spectrum also called Loève spectrum. An estimation procedure of the Loève spectrum was suggested in Soedjak (Soedjak), but in order to capture enough of the complexity of the brain mechanisms these results have to be properly extended. This was achieved in a recent and important contribution due to Gorrostieta et al. (2019). They follow the approach of Dahlhaus (Dahlhaus) to introduce multivariate locally-harmonizable processes. They describe a windowed Fourier based estimation procedure of the time-varying dual-frequency coherence. They derive exact confidence intervals for testing if the coherence differs from zero under iid Gaussian assumptions and also obtain asymptotic confidence intervals.

In this paper, we introduce a class of spatio-temporal processes that are locally time-harmonizable. We consider available replicates and seek for the estimation of both the Spatial Time-Varying Loève-spectrum and the Spatial Time-Varying Dual-Frequency coherence function (hereafter STV Loève spectrum and STVDF coherence function respec-

tively). In other words we measure a time evolutionary squared correlation coefficient across different frequencies between any pairs of spatial locations. Our method exploits the spatial correlations in order to improve the location specific estimation of these quantities in the spirit of Ombao et al. (2008). In order to construct proper confidence intervals for the STVDF coherence function, we adapt the Circular Block Bootstrap method and show its consistency.

We apply our method to real data set coming from an experiment designed to test the performance of visual working memory of subjects. In this experiment, the distribution of the response variables describing the memorization performance of patients is properly modeled through a toroidal mixture which serves us for unsupervised classification of the subject-specific replicates. Within each of these labeled replicates we estimate the corresponding STVDF coherence functions. The final stage of our method is to build from the STVDF coherence functions dynamic functional connectivity networks. It allows us to notably reveal that connectivity within the prefrontal cortex in between the alpha-beta frequency bands during the first stage of experiment is associated to better spatial and color memorization performance. The computational complexity of our method can be reasonably tackled considering the nature of our real data and by a two-step approach which consists in using bootstrap in anatomical regions and time laps of interest only, that is, wherever the coherence function is above a user predefinite threshold.

The contribution of this paper is two-fold. First, from neuroscientists point of view, we propose a coherent data analysis pipeline which could be easily adapt to other similar experiments. We illustrate that there may be some interesting information in the dual-frequency coherence which can help to understand the VWM brain mechanisms. Second, from a statistical point of view, we unify and generalize the two important contributions

of Ombao et al. (2008); Gorrostieta et al. (2019).

The paper is organized as follows. In an introductory section we recall the basics of coherence analysis for multivariate stationary and harmonizable time series. In Section 3 we introduce the spatial and locally time-harmonizable time series model along with a proper estimation procedure under realistic modeling assumptions. In Section 4 we apply our method to a real data set.

2 Review of coherence analysis for multivariate time series

Hereafter the symbol $(\cdot)'$ denotes the transpose of a vector. The spectral or Cramer's representation of a centered P-variate discrete-time stationary process $\{\boldsymbol{X}_t,\ t \in \mathbb{Z}\}$, where $\boldsymbol{X}_t = (X_t^{(1)}, \ldots, X_t^{(P)})'$, is given by the following Fourier-Stieltjes integral (Brockwell and Davis, 1991)

$$\boldsymbol{X}_t = \int_{-\pi}^{\pi} e^{it\omega} d\boldsymbol{Z}\left(\omega\right),$$

where $\left\{\boldsymbol{Z}(\omega) = (Z^{(1)}(\omega), \ldots, Z^{(P)}(\omega))',\ \omega \in [-\pi, \pi)\right\}$ is a zero-mean stochastic process with orthogonal and cross-orthogonal increments $\left\{dZ^{(j)}\left(\omega\right); j = 1, \ldots, P,\ \omega \in [-\pi, \pi)\right\}$. Moreover,

$$\mathrm{Cov}(d\boldsymbol{Z}(\omega_1), d\boldsymbol{Z}(\omega_2)) = \delta(\omega_1 - \omega_2)\boldsymbol{f}(\omega_1)d\omega_1 d\omega_2,$$

where $\boldsymbol{f}$ is the $P \times P$ spectral density matrix and $\delta(\omega_1 - \omega_2)$ the Dirac-delta function.

The squared coherence can be defined in terms of spectral density or of the incremental process as follows:

$$\rho^{(pq)}(\omega) := \frac{\mathrm{Cov}\left(dZ^{(p)}(\omega), dZ^{(q)}(\omega)\right)}{\left\{\mathrm{Var}\left(dZ^{(p)}(\omega)\right)\mathrm{Var}\left(dZ^{(q)}(\omega)\right)\right\}^{1/2}} = \frac{\left|f^{(pq)}(\omega)\right|^2}{\left\{f^{(pp)}(\omega) f^{(qq)}(\omega)\right\}^{1/2}} \quad (1)$$

This quantity is a correlation of the global oscillatory behavior at a frequency ω between the vector components p and q. We see that within the class of stationary processes, we cannot capture the cross-oscillatory behavior between different frequency bands. The class of (strongly) harmonizable processes is required. This is a more general class than the one of stationary processes (Loève, 1948; Rozanov, 1959; Cramér, 1961) and it contains for instance periodically correlated processes (Hurd and Miamee, 2007).

The spectral representation of harmonizable process $\{\boldsymbol{X}_t,\ t \in \mathbb{Z}\}$ is given by

$$\boldsymbol{X}_t = \int_{-\pi}^{\pi} e^{it\omega} d\boldsymbol{Z}(\omega),$$

where $d\boldsymbol{Z}(\omega) = \left(dZ^{(1)}, \ldots, dZ^{(P)}\right)'$ is a random vector process with zero mean and possibly correlated increments. Moreover,

$$\mathrm{Cov}(dZ^{(p)}(\omega_1), dZ^{(q)}(\omega_2)) = f^{(pq)}(\omega_1, \omega_2) d\omega_1 d\omega_2,$$

where $f^{(pq)}(\omega_1, \omega_2)$ is known as the Loève spectrum.

The dual frequency coherence between a pair of time series $\left\{X^{(p)}, X^{(q)},\ t \in \mathbb{Z}\right\}$ and a pair of frequencies (ω_1, ω_2) is defined as

$$\begin{aligned} \rho^{(pq)}(\omega_1, \omega_2) &:= \frac{\mathrm{Cov}\left(dZ^{(p)}(\omega_1), dZ^{(q)}(\omega_2)\right)}{\left\{\mathrm{Var}\left(dZ^{(p)}(\omega_1)\right)\mathrm{Var}\left(dZ^{(q)}(\omega_2)\right)\right\}^{1/2}} \\ &= \frac{\left|f^{(pq)}(\omega_1, \omega_2)\right|^2}{f^{(pp)}(\omega_1, \omega_1) f^{(qq)}(\omega_2, \omega_2)}. \end{aligned}$$

Note that the dual-frequency coherence given by the previous equation is constant in time. In the next section we propose a proper model to capture spatial and dynamic behaviors of the dual-frequency coherence function.

3 Spatial time-varying dual-frequency coherence estimation

In this section we unify and extend the work of Ombao et al. (2008); Gorrostieta et al. (2019). For the sake of clarity, we first introduce the spatial time-harmonizable processes before giving their locally time-harmonizable version. We define the corresponding spatial time-varying Loève spectrum and spatial time-varying dual-frequency coherence function. Then we set-up our modeling assumptions, in particular the space-time rescaling which enables for infill asymptotic theory. We construct the estimator of the spatial time-varying dual-frequency coherence and derive its asymptotic performances. Finally we show how to adapt the CBB method to build bootstrap confidence intervals and we prove the bootstrap consistency.

3.1 Location dependent Loève spectrum

Let $\left\{\boldsymbol{X}_t^{\underline{S}}\right\} = \left\{\boldsymbol{X}_t^{\underline{S}}, t \in \mathbb{Z}\right\} := \left\{X_t^{\underline{S}}(\underline{s}), t \in \mathbb{Z}, \underline{s} \in \{1, \ldots, S_1\} \times \{1, \ldots, S_2\}\right\}$, $\underline{S} := (S_1, S_2) \in \{1, \ldots\} \times \{1, \ldots\}$, be a family of spatial (location-dependent) time-harmonizable processes, i.e.,

$$X_t^{\underline{S}}(\underline{s}) = \int_{-\pi}^{\pi} e^{-i\omega t} dZ_{\underline{s}}^{\underline{S}}(\omega)\,,$$

such that

$$\mathrm{Cov}\left(dZ^{\underline{S}}_{\underline{s}_1}(\omega_1), dZ^{\underline{S}}_{\underline{s}_2}(\omega_2)\right) = f^{\underline{S}}_{\underline{s}_1,\underline{s}_2}(\omega_1,\omega_2)\, d\omega_1 d\omega_2,$$

where $f^{\underline{S}}_{\underline{s}_1,\underline{s}_2}(\omega_1,\omega_2)$ is the spatial Loève spectrum.
We observe the process $X^{\underline{S}}_t(\underline{s})$ for $t = 1,\ldots,T$ in $S_1 \times S_2$ different locations, i.e. s_1 and s_2 can take S_1 and S_2 different values, respectively: $s_i = 1,\ldots,S_i$ for $i = 1,2$.

Notice that a sufficient condition for time-harmonizability and existence of a two-dimensional spectral density for second order spatial random processes is

$$\sum_{(t_1,t_2)\in\mathbb{Z}^2} \left|C^{\underline{S}}_{\underline{s}_1,\underline{s}_2}(t_1,t_2)\right| < \infty,$$

where $C^{\underline{S}}_{\underline{s}_1,\underline{s}_2}(t_1,t_2) = \mathrm{Cov}\left(X^{\underline{S}}_{t_1}(\underline{s}_1), X^{\underline{S}}_{t_2}(\underline{s}_2)\right)$.
Then the Loève spectrum is a continuous function and it coincides with

$$f^{\underline{S}}_{\underline{s}_1,\underline{s}_2}(\omega_1,\omega_2) = \frac{1}{4\pi^2}\sum_{(t_1,t_2)\in\mathbb{Z}^2} C^{\underline{S}}_{\underline{s}_1,\underline{s}_2}(t_1,t_2)\, e^{-i(\omega_1 t_1 - \omega_2 t_2)}.$$

Since we observe the time series on $[0,T]$, we are going to estimate

$$f^{+,\underline{S}}_{\underline{s}_1,\underline{s}_2}(\omega_1,\omega_2) := \frac{1}{4\pi^2}\sum_{(t_1,t_2)\in\mathbb{N}^2} C^{\underline{S}}_{\underline{s}_1,\underline{s}_2}(t_1,t_2)\, e^{-i(\omega_1 t_1 - \omega_2 t_2)}.$$

Then for $t_1, t_2 \geq 0$,

$$C^{\underline{S}}_{\underline{s}_1,\underline{s}_2}(t_1,t_2) = \int_{-\pi}^{\pi}\int_{-\pi}^{\pi} f^{+,\underline{S}}_{\underline{s}_1,\underline{s}_2}(\omega_1,\omega_2)\, e^{i(\omega_1 t_1 - \omega_2 t_2)} d\omega_1 d\omega_2.$$

Let $C^{+,\underline{S}}_{\underline{s}_1,\underline{s}_2}(t_1,t_2) := C_{\underline{s}_1,\underline{s}_2}(t_1,t_2)$ for $t_1,t_2 \geq 0$, and $C^{+,\underline{S}}_{\underline{s}_1,\underline{s}_2}(t_1,t_2) = 0$ otherwise.
For the purpose our application we have to make this spatial process locally time-harmonizable to account for possible changes in the Loève spectrum over the time and therefore in the dual-frequency coherence function.

3.2 Location dependent time-varying Loève spectrum

We consider a spectral representation of $X_t^{T,\underline{S}}$ based on an unknown and finite number of Fourier frequencies of the form $\omega_k^{(M)} = \pi k/M,\ -M \leq k < M$:

$$X_t^{T,\underline{S}} = \sum_{k=-M}^{M-1} \exp\left(-i\omega_k^{(M)} t\right) \Delta Z_t^{M,T,\underline{S}}(\omega_k^{(M)}), \tag{2}$$

where

$$\mathrm{Cov}\left(\Delta Z_{t_1,\underline{s}_1}^{M,T,\underline{S}}(\omega_1), \Delta Z_{t_2,\underline{s}_2}^{M,T,\underline{S}}(\omega_2)\right) \approx f_{t_1,t_2,\underline{s}_1,\underline{s}_2}^{T,\underline{S}}(\omega_1,\omega_2)\,\Delta\omega_1\Delta\omega_2$$

and $f_{t_1,t_2,\underline{s}_1,\underline{s}_2}^{T,\underline{S}}(\omega_1,\omega_2)$ is the time-varying spatial Loève spectrum.

This modeling choice, given by the equation (2), is motivated by our real data application for which we typically consider a finite number of frequency bands of interest. Moreover, it will become clear hereafter that this choice allows us to keep more tractable the multiple asymptotic theory of Section 3.5.

$$\begin{aligned} f_{t_1,t_2,\underline{s}_1,\underline{s}_2}^{T,\underline{S},M}(\omega_1,\omega_2) &:= \frac{1}{4\pi^2} \sum_{k_1=t_1-M}^{t_1+M-1} \sum_{k_2=t_2-M}^{t_2+M-1} C_{\underline{s}_1,\underline{s}_2}^{T,\underline{S}}(k_1,k_2)\, e^{-i(\omega_1 k_1 - \omega_2 k_2)} \\ &= \frac{1}{4\pi^2} \sum_{k_1=-M}^{M-1} \sum_{k_2=-M}^{M-1} C_{\underline{s}_1,\underline{s}_2}^{T,\underline{S}}(t_1+k_1,t_2+k_2)\, e^{-i(\omega_1 k_1 - \omega_2 k_2)} e^{-i(\omega_1 t_1 - \omega_2 t_2)}, \end{aligned} \tag{3}$$

where $C_{\underline{s}_1,\underline{s}_2}^{T,\underline{S}}(k_1,k_2) := \mathrm{E}\left(X_{k_1}^{T,\underline{S}_1}(\underline{s}) X_{k_2}^{T,\underline{S}_2}(\underline{s})\right)$.

Then we readily obtain that

$$C_{\underline{s}_1,\underline{s}_2}^{T,\underline{S}}(t_1,t_2) = \frac{\pi^2}{N^2} \sum_{j_1=-M}^{M-1} \sum_{j_2=-M}^{M-1} f_{t_1,t_2,\underline{s}_1,\underline{s}_2}^{T,\underline{S},M}\left(\omega_{j_1}^{(M)}, \omega_{j_2}^{(M)}\right) e^{i\left(\omega_{j_1}^{(M)} t_1 - \omega_{j_2}^{(M)} t_2\right)}, \tag{4}$$

where $\omega_j^{(M)} = \frac{\pi j}{M},\ j = -M,\ldots,M-1$, denote the Fourier frequencies of the observations. Notice that $\frac{\pi}{M}$ is the increment between two consecutive Fourier frequencies :

$\omega_{j+1}^{(M)} - \omega_j^{(M)} = \frac{\pi}{M}$.

3.3 Assumptions

In the following we state our modeling assumptions. Our observations consist in sampled and replicated time-spatial random arrays

$$\left\{ \boldsymbol{X}_t^{\underline{S},r} : t = 0, \dots, T;\ r = 1, \dots, R,\ \underline{S} := (S_1, S_2) \in \{1, \dots\} \times \{1, \dots\} \right\}.$$

The location dependent time-varying Loève spectrum $f_{t_1,t_2,\underline{s}_1,\underline{s}_2}^{T,\underline{S},N}(\omega_1, \omega_2)$ defined by the equation (3) is rescaled in space and in time. Hereafter, we denote as $f_{\tau_1,\tau_2,\underline{u}_1,\underline{u}_2}(\omega_1, \omega_2)$ the **rescaled spatio-temporal Loève spectrum**, where $\underline{u}_1, \underline{u}_2 \in [0,1]^2$ and $\tau_1, \tau_2 \in [0,1]$.

We define $\ddot{\underline{s}} := (\ddot{s}_1, \ddot{s}_2) = \left(\frac{s_1}{S_1}, \frac{s_2}{S_2}\right)$ for $\underline{s} = (s_1, s_2) \in \{1, \dots, S_1\} \times \{1, \dots, S_2\}$. For $\underline{u} \in [0,1]^2$ denote $\underline{u} \sim \ddot{\underline{s}}$ when $\underline{s} = (\lfloor u_1 S_1 \rfloor, \lfloor u_2 S_2 \rfloor)$ and $\ddot{t} := \frac{t}{T}$ for $t \in \{1, \dots, T\}$. For $\tau \in [0,1]$ denote $\tau \sim \ddot{t}$ when $t = \lfloor \tau T \rfloor$.

We assume the following conditions:

(L) There exists a function $f : [0,1]^6 \times [-\pi, \pi)^2 \to \mathbb{C}$ which is Lipschitz-continuous with respect to the space and the time components uniformly on the frequency components, that is there exists some constant $L > 0$ such that for each $\underline{u}_1, \underline{u}_2, \underline{u}_3, \underline{u}_4, \in [0,1]^2$, $\tau_1, \tau_2 \in [0,1]$ and each $\omega_1, \omega_2 \in [-\pi, \pi)$,

$$\left| f_{\tau_1,\tau_2,\underline{u}_1,\underline{u}_2}(\omega_1, \omega_2) - f_{\tau_3,\tau_4\underline{u}_3,\underline{u}_4}(\omega_1, \omega_2) \right| \leq L \left(|\tau_1 - \tau_3| + |\tau_2 - \tau_4| + \|\underline{u}_1 - \underline{u}_3\| + \|\underline{u}_2 - \underline{u}_4\| \right), \tag{5}$$

and there exists some constant $Q > 0$ such that

$$\left| f^{T,\underline{S},N}_{t_1,t_2,\underline{s}_1,\underline{s}_2}(\omega_1,\omega_2) - f_{\ddot{t}_1,\ddot{t}_2,\ddot{\underline{s}}_1,\ddot{\underline{s}}_2}(\omega_1,\omega_2) \right| \leq \frac{Q}{S_1 S_2 T}, \tag{6}$$

where $\underline{s}_i = (s_{i,1}, s_{i,2})$, $\ddot{\underline{s}}_i = (s_{i,1}/S_1, s_{i,2}/S_2), \ddot{t}_i = t_i/T, i = 1, 2$.

(F) We consider a finite number $(2M)$ of frequencies in equation (2) which are Fourier frequencies : $\omega_i = \frac{\pi k_i}{M}$, $k_1 = -M, \ldots, M-1$, $i = 1, 2$.

(M) We let $\{X^{\underline{S},r}_t(\underline{s})\}$ be α-mixing with respect to the replicates, i.e., $\alpha_X(k) \to 0$ as $k \to \infty$, where

$$\alpha_X(k) = \sup_k \sup_{\substack{A \in \mathcal{F}_X(1,r) \\ B \in \mathcal{F}_X(r+k,\infty)}} |P(A \cap B) - P(A)P(B)|$$

and $\mathcal{F}_X(1,r) = \sigma\left(\{X^{\underline{S},q}_t(\underline{s}) : q \leq r, t \in \mathbb{Z} \text{ and all locations } \underline{s}\}\right)$,
$\mathcal{F}_X(r+k,\infty) = \sigma\left(\{X^{\underline{S},q}_t(\underline{s}) : q \geq r+k, t \in \mathbb{Z} \text{ and all locations } \underline{s}\}\right)$.

α-mixing is a weak dependence measure. Hence, replicated time-series closed to each other in time can be dependent while when they are far away they are almost independent. This generalizes the modeling assumptions of Gorrostieta et al. (2019). For properties and examples of other dependence measures, we refer the reader to (Doukhan, 1994).

(B) Boundedness :

(i) either, there exists some constant $C > 0$ such that $\sup_{t,r,\underline{s}} \left| X^{\underline{S},r}_t(\underline{s}) \right| \leq C$ and $\sum_r \alpha(r) < \infty$,

(ii) or, for some $\delta > 0$, $\sup_{t,r,\underline{s}} \mathrm{E}\left(\left| X^{\underline{S},r}_t(\underline{s}) \right|^{4+\delta} \right) < \infty$ and $\sum_r \alpha(r)^{\delta/(4+\delta)} < \infty$.

This assumption is used to prove the convergence of second order moment of our estimator. In order to prove asymptotic normality of our estimator we state the following additional assumptions.

(GR) The time-spatial random array

$$\left\{X_t^{T,\underline{S},r}(\underline{s}) : t \in \{0,\dots,T\}, \underline{s} \in \{1,\dots,S_1\} \times \{1,\dots,S_2\}, r = 1,\dots,R\right\}$$

is Gaussian for any $R > 0$.

(**LR**) There exists a family of functions $f^{r_1,r_2} : [0,1]^2 \times [0,1]^4 \times [-\pi,\pi)^2 \to \mathbb{C}$, $r_1, r_2 \in \mathbb{N}$, which are Lipschitz-continuous with respect to the space and the time components uniformly on the frequency components and to the index (r_1, r_2), that is there exists some constant $L > 0$ such that for each $\tau_1, \tau_2, \tau_3, \tau_4 \in [0,1]$, each $\underline{u}_1, \underline{u}_2, \underline{u}_3, \underline{u}_4 \in [0,1]^2$ and each $\omega_1, \omega_2 \in [-\pi, \pi)$,

$$\left|f^{r_1,r_2}_{\tau_1,\tau_2,\underline{u}_1,\underline{u}_2}(\omega_1,\omega_2) - f^{r_1,r_2}_{\tau_3,\tau_4,\underline{u}_3,\underline{u}_4}(\omega_1,\omega_2)\right| \leq L\left(|\tau_1-\tau_3| + |\tau_2-\tau_4| + \|\underline{u}_1-\underline{u}_3\| + \|\underline{u}_2-\underline{u}_4\|\right), \tag{7}$$

And there exists some constant $Q > 0$ such that

$$\left|f^{T,\underline{S},N,r_1,r_2}_{t_1,t_2,\underline{s}_1,\underline{s}_2}(\omega_1,\omega_2) - f^{r_1,r_2}_{\ddot{t}_1,\ddot{t}_2,\ddot{\underline{s}}_1,\ddot{\underline{s}}_2}(\omega_1,\omega_2)\right| \leq \frac{Q}{S_1 S_2 T}, \tag{8}$$

where $\underline{s}_i = (s_{i,1}, s_{i,2})$ and $\ddot{\underline{s}}_i = (s_{i,1}/S_1, s_{i,2}/S_2), i = 1, 2$.

When $r_1 = r_2 = r$ we denote $\qquad f^{r,r}_{\tau_1,\tau_2,\underline{u}_1,\underline{u}_2}(\omega_1,\omega_2) = f^{r}_{\tau_1,\tau_2,\underline{u}_1,\underline{u}_2}(\omega_1,\omega_2)$.

Note that the constants L and Q do not depend on $r_1, r_2, \underline{s}_1, \underline{s}_2, \underline{u}_1, \underline{u}_2, \omega_1, \omega_2$ and can be different from the constants given in condition **(LR)**.

(**SR**) Stationarity with respect to the replications (replications are stationary with respect to r). We have

$$f^{r+k,r}_{\tau_1,\tau_2,\underline{u}_1,\underline{u}_2}(\omega_1,\omega_2) = f^{k,0}_{\tau_1,\tau_2,\underline{u}_1,\underline{u}_2}(\omega_1,\omega_2) := f^{k}_{\tau_1,\tau_2,\underline{u}_1,\underline{u}_2}(\omega_1,\omega_2)$$

for each $k \in \mathbb{Z}$ and each non negative number $r \geq -k$.

Note that the condition (**LR**) is a generalization of condition (**L**) accross replicates.

3.4 Construction of the estimator

In this section we build an estimation procedure for the rescaled spatio-temporal Loève spectrum $f_{\tau_1,\tau_2,\underline{u}_1,\underline{u}_2}(\omega_1,\omega_2)$. We define $w_{\underline{u}}(\underline{s})$ the two-dimensional kernel function which allows us to rescale in space and the one-dimensional kernel function $W_\tau(\cdot)$ that acts as a window for time localization. For simplicity we consider over space an isotropic kernel of the form

$$w_{\underline{u}}(\underline{s}) := w_{u_1}(s_1)w_{u_2}(s_2),$$

where $\underline{u} = (u_1, u_2)$ and $\underline{s} = (s_1, s_2)$ and

$$w_u(s_i) := \frac{1}{S_i h} w\left(\frac{u_i - s_i/S_i}{h}\right),$$

for $u \in (0,1)$, $h \to 0$ as $S_1, S_2 \to \infty$. Moreover, the window for time localization is of the form

$$W_\tau(t) := \frac{1}{T\hbar} W\left(\frac{\tau - t/T}{\hbar}\right),$$

for $\tau \in (0,1)$, $\hbar \to 0$ as $T \to \infty$.

We assume that the kernel functions $w(\cdot) : \mathbb{R} \to [0,\infty)$ and $W_\tau(\cdot)$ are symmetric non-negative with support contained in $[-1,1]$ and such that $\int_{-1}^{1} w(u)du = 1$ and $\int_{-1}^{1} W(u)du =$

1. Moreover we assume that they are piecewise Lipschitz-continuous in the sense that there exist $k, k' \in \mathbb{N}$, $u_1, \ldots, u_k \in [-1, 1]$ and $\tau_1, \ldots, \tau_{k'} \in [-1, 1]$ such that $w(\cdot)$ and $W(\cdot)$ are Lipschitz-continuous on each interval (u_j, u_{j+1}); $1 \leq j \leq k-1$ and $(\tau_{j'}, \tau_{j'+1})$; $1 \leq j' \leq k'-1$, respectively.

We define the dual-frequency periodogram of the r-th replicate between times t_1 and t_2, spatial locations $\underline{s}_1, \underline{s}_2$, at frequencies ω_1, ω_2 and over a time-window of size N as

$$I^{T,\underline{S},N,r}_{t_1,t_2,\underline{s}_1,\underline{s}_2}(\omega_1, \omega_2) := \frac{1}{4\pi^2} d^{T,\underline{S},N,r}_{t_1,\underline{s}_1}(\omega_1)\, \overline{d^{T,\underline{S},N,r}_{t_2,\underline{s}_2}(\omega_2)},$$

where

$$d^{T,\underline{S},N,r}_{t,\underline{s}}(\omega) := \sum_{k=t-N}^{t+N-1} X^{T,\underline{S},r}_k(\underline{s})\, e^{-i\omega k} = \sum_{k=-N}^{N-1} X^{T,\underline{S},r}_{k+t}(\underline{s})\, e^{-i\omega(k+t)}$$

is the Fourier transform of the r-th replicate at location $\underline{s}$ and time moment t.

In order to estimate the time-varying Loève spectrum, we considered (local) windows around the time points of interest. We define the time-varying Loève spectrum of the observations $X^{T,\underline{S}}_t(\underline{s})$ by taking the window length equal to an integer multiple of M in order to ensure the identifiability of the frequencies.

Let

$$\hat{f}^{T,\underline{S},N,R}_{t_1,t_2,\underline{s}_1,\underline{s}_2}(\omega_1, \omega_2) := \frac{1}{R} \sum_{r=1}^{R} I^{T,\underline{S},N,r}_{t_1,t_2,\underline{s}_1,\underline{s}_2}(\omega_1, \omega_2)\,.$$

The estimator of $f_{\tau_1,\tau_2,\underline{u}_1,\underline{u}_2}(\omega_1, \omega_2)$ is defined as follows

$$\widetilde{f}^{T,\underline{S},N,R}_{\tau_1,\tau_2,\underline{u}_1,\underline{u}_2}(\omega_1, \omega_2) := \sum_{t_1} \sum_{t_2} \sum_{\underline{s}_1} \sum_{\underline{s_2}} W_{\tau_1}(t_1) W_{\tau_2}(t_2) w_{\underline{u}_1}(\underline{s}_1) w_{\underline{u}_2}(\underline{s}_2) \hat{f}^{T,\underline{S},N,R}_{t_1,t_2,\underline{s}_1,\underline{s}_2}(\omega_1, \omega_2)\,.$$

From now on, for the sake of simplicity, when there is no possibility of confusion, we denote $\widetilde{f}^{T,\underline{S},N,R}_{\tau_1,\tau_2,\underline{u}_1,\underline{u}_2}(\omega_1, \omega_2)$ by $\widetilde{f}^{R}_{1,2}(\omega_1, \omega_2)$, and $f_{\tau_1,\tau_2,\underline{u}_1,\underline{u}_2}(\omega_1, \omega_2)$ by $f_{1,2}(\omega_1, \omega_2)$. Moreover,

let us denote

$$\begin{aligned}\widetilde{d}_i^r(\omega) &= \widetilde{d}^{T,\underline{S},N,r}_{\tau_i,\underline{u}_i}(\omega) := \sum_{t_i}\sum_{\underline{s}_i} W_{\tau_i}(t_i) w_{\underline{u}_i}(\underline{s}_i) d^{T,\underline{S},r}_{t_i,\underline{s}_i}(\omega) \\ &= \sum_{t_i}\sum_{\underline{s}_i} W_{\tau_i}(t_i) w_{\underline{u}_i}(\underline{s}_i) \sum_{k_i=t_i-N}^{t_i+N-1} X_{k_i}^{T,\underline{S},r}(\underline{s}_i)\, e^{-i\omega k_i},\end{aligned}$$

where $i = 1, 2$. Then the estimator $\widetilde{f}^R_{1,2}(\omega_1, \omega_2)$ can be equivalently expressed as

$$\widetilde{f}^R_{1,2}(\omega_1,\omega_2) = \frac{1}{R}\sum_{r=1}^{R} \widetilde{I}^{T,\underline{S},N,r}_{\tau_1,\tau_2,\underline{u}_1,\underline{u}_2}(\omega_1,\omega_2) = \frac{1}{4\pi^2 R}\sum_{r=1}^{R} \widetilde{d}_1^r(\omega_1)\,\overline{\widetilde{d}_2^r(\omega_2)}, \tag{9}$$

where the space and time smoothed periodogram $\widetilde{I}^{T,\underline{S},N,r}_{\tau_1,\tau_2,\underline{u}_1,\underline{u}_2}(\omega_1,\omega_2)$ is defined by

$$\widetilde{I}^r_{1,2}(\omega_1,\omega_2) = \widetilde{I}^{T,\underline{S},N,r}_{\tau_1,\tau_2,\underline{u}_1,\underline{u}_2}(\omega_1,\omega_2) := \frac{1}{4\pi^2}\widetilde{d}_1^r(\omega_1)\,\overline{\widetilde{d}_2^r(\omega_2)}. \tag{10}$$

The rescaled time-varying spatial coherence is defined as

$$\rho_{\tau_1,\tau_2,\underline{u}_1,\underline{u}_2}(\omega_1,\omega_2) := \frac{\left|f_{\tau_1,\tau_2,\underline{u}_1,\underline{u}_2}(\omega_1,\omega_2)\right|^2}{f_{\tau_1,\tau_1,\underline{u}_1,\underline{u}_1}(\omega_1,\omega_1)\, f_{\tau_2,\tau_2,\underline{u}_2,\underline{u}_2}(\omega_2,\omega_2)}, \tag{11}$$

and its estimator is of the form

$$\widetilde{\rho}^{T,\underline{S},N,R}_{\tau_1,\tau_2,\underline{u}_1,\underline{u}_2}(\omega_1,\omega_2) := \frac{\left|\widetilde{f}^{T,\underline{S},N,R}_{\tau_1,\tau_2,\underline{u}_1,\underline{u}_2}(\omega_1,\omega_2)\right|^2}{\widetilde{f}^{T,\underline{S},N,R}_{\tau_1,\tau_1,\underline{u}_1,\underline{u}_1}(\omega_1,\omega_1)\,\widetilde{f}^{T,\underline{S},N,R}_{\tau_2,\tau_2,\underline{u}_2,\underline{u}_2}(\omega_2,\omega_2)}. \tag{12}$$

3.5 Asymptotic properties

In the sequel, we exhibit some important properties of our estimation procedure starting with the convergence in quadratic mean and the asymptotic normality. All the proofs are deferred to the companion document.

In the following any complex number z is treated as a vector of its real and imaginary parts, i.e., $z = (\Re z, \Im z)'$.

3.5.1 Convergence in quadratic mean

Theorem 3.1. *(Convergence in quadratic mean)*
Under conditions (F), (LC), (M) and (B) the estimator $\widetilde{f}^{T,\underline{S},N,R}_{\tau_1,\tau_2,\underline{u}_1,\underline{u}_2}(\omega_1,\omega_2)$ *(see equation (9)) satisfies*

$$\lim_{R\to\infty} \widetilde{f}^{T,\underline{S},N,R}_{\tau_1,\tau_2,\underline{u}_1,\underline{u}_2}(\omega_1,\omega_2) = f_{\tau_1,\tau_2,\underline{u}_1,\underline{u}_2}(\omega_1,\omega_2) \qquad \textit{in quadratic mean,}$$

for $\omega_i = \frac{\pi k_i}{M}$, $k_1 = -M,\ldots,M-1$, $i=1,2$, *provided that* $N = nM$, *as well as* $R^{-1}N^4, (S_1+S_2)h^2, T\hbar^2 \to \infty$, $n^2(S_1S_2T)^{-1} \to 0$ *and* $n^2(h+\hbar), n^3T^{-1} \to 0$ *as* $T, S_1, S_2 \to \infty$, $h, \hbar \to 0$ *independently of the behavior of* $n > 1$.

Lemma 3.1. *Assume that conditions (LR), (SR) and (F) are satisfied as well as the condition*

$$\sum_{k\in\mathbb{Z}} \left| f^k_{\tau_j,\tau_{j'},\underline{u}_j,\underline{u}_{j'}}(\omega_j,\omega_{j'}) \right| < \infty.$$

Then,

$$\begin{aligned}
&\lim_{R\to\infty} R\mathrm{Cov}\left(\widetilde{f}^R_{1,2}(\omega_1,\omega_2), \widetilde{f}^R_{3,4}(\omega_3,\omega_4)\right) \\
&\quad = \sum_{k\in\mathbb{Z}} \left(f^k_{\tau_1,\tau_3,\underline{u}_1,\underline{u}_3}(\omega_1,\omega_3) f^k_{\tau_2,\tau_4,\underline{u}_2,\underline{u}_4}(-\omega_2,-\omega_4) + f^k_{\tau_1,\tau_4,\underline{u}_1,\underline{u}_4}(\omega_1,-\omega_4) f^k_{\tau_2,\tau_3,\underline{u}_2,\underline{u}_3}(-\omega_2,\omega_3)\right)
\end{aligned}$$

for any ω_j, τ_j, $j = 1,\ldots,4$ *and for any rescaled spatial locations* $\underline{u}_1,\ldots,\underline{u}_4$, *provided that*

$$RN^2\left(\frac{1}{S_1S_2T} + h + \hbar + \frac{N}{T}\right) \to 0, \ \ R, S_1, S_2, T \to \infty.$$

Thus, we have,

$$\begin{aligned}
&\lim_{R\to\infty} R\mathrm{Var}\left(\widetilde{f}^R_{1,2}(\omega_1,\omega_2)\right) \\
&\quad = \sum_{k\in\mathbb{Z}} \left(f^k_{\tau_1,\tau_1,\underline{u}_1,\underline{u}_2}(\omega_1,\omega_1) f^k_{\tau_2,\tau_2,\underline{u}_2,\underline{u}_2}(-\omega_2,-\omega_2) + f^k_{\tau_1,\tau_4,\underline{u}_1,\underline{u}_2}(\omega_1,-\omega_2) f^k_{\tau_2,\tau_1,\underline{u}_2,\underline{u}_1}(-\omega_2,\omega_1)\right)
\end{aligned}$$

From the equality (9) and because the observed process $\left\{\boldsymbol{X}_t^{\underline{S}}\right\}$ is real-valued, we remark that $\overline{\widetilde{f}_{1,2}^R(\omega_1,\omega_2)}$ coincides with $\widetilde{f}_{1,2}^R(-\omega_1,-\omega_2)$ and

$$\begin{aligned}\Re\widetilde{f}_{1,2}^R(\omega_1,\omega_2) &= \frac{1}{2}\left(\widetilde{f}_{1,2}^R(\omega_1,\omega_2)+\widetilde{f}_{1,2}^R(-\omega_1,-\omega_2)\right)\\ \Im\widetilde{f}_{1,2}^R(\omega_1,\omega_2) &= \frac{1}{2i}\left(\widetilde{f}_{1,2}^R(\omega_1,\omega_2)-\widetilde{f}_{1,2}^R(-\omega_1,-\omega_2)\right).\end{aligned}$$

Then we can compute the elements of the covariance matrix of $\widetilde{f}_{1,2}^R(\omega_1,\omega_2)$. Hence

$$\begin{aligned}&\mathrm{Var}\left(\Re\widetilde{f}_{1,2}^R(\omega_1,\omega_2)\right)=\frac{1}{2}\left(\mathrm{Var}\left(\widetilde{f}_{1,2}^R(\omega_1,\omega_2)\right)+\Re\mathrm{Cov}\left(\widetilde{f}_{1,2}^R(\omega_1,\omega_2),\widetilde{f}_{1,2}^R(-\omega_1,-\omega_2)\right)\right),\\ &\mathrm{Cov}\left(\Re\widetilde{f}_{1,2}^R(\omega_1,\omega_2),\Im\widetilde{f}_{1,2}^R(\omega_1,\omega_2)\right)=\frac{1}{2}\Im\mathrm{Cov}\left(\widetilde{f}_{1,2}^R(\omega_1,\omega_2),\widetilde{f}_{1,2}^R(-\omega_1,-\omega_2)\right),\\ &\mathrm{Var}\left(\Im\widetilde{f}_{1,2}^R(\omega_1,\omega_2)\right)=\frac{1}{2}\left(\mathrm{Var}\left(\widetilde{f}_{1,2}^R(\omega_1,\omega_2)\right)-\Re\mathrm{Cov}\left(\widetilde{f}_{1,2}^R(\omega_1,\omega_2),\widetilde{f}_{1,2}^R(-\omega_1,-\omega_2)\right)\right).\end{aligned}$$

These formulas and the Lemma 3.1 are used to derive the form of the covariance matrix of the limit distribution of $\sqrt{R}\widetilde{f}_{1,2}^R(\omega_1,\omega_2)$ as $R\to\infty$.

Let us introduce some additional notations that we use to formulate the multivariate central limit theorem hereafter

$$\begin{aligned}\tilde{\boldsymbol{f}}^{T,\underline{S},N,R} &:= \left(\left(\widetilde{f}^{T,\underline{S},N,R}_{\tau_{1,1},\tau_{2,1},\underline{u}_{1,1},\underline{u}_{2,1}}(\omega_{1,1},\omega_{2,1})\right)',\ldots,\left(\widetilde{f}^{T,\underline{S},N,R}_{\tau_{1,k},\tau_{2,k},\underline{u}_{1,k},\underline{u}_{2,k}}(\omega_{1,k},\omega_{2,k})\right)'\right)',\\ \boldsymbol{f} &:= \left(\left(f_{\tau_{1,1},\tau_{2,1},\underline{u}_{1,1},\underline{u}_{2,1}}(\omega_{1,1},\omega_{2,1})\right)',\ldots,\left(f_{\tau_{1,k},\tau_{2,k},\underline{u}_{1,k},\underline{u}_{2,k}}(\omega_{1,k},\omega_{2,k})\right)'\right)',\end{aligned}$$

where k is some positive integer and $\tau_{j,l}\in[0,1],\underline{u}_{j,l}\in[0,1]^2,\omega_{j,l}\in(-\pi,\pi]$, $j=1,2,l=1,\ldots,k$.

Theorem 3.2. *Assume that the time-spatial random arrays* $\left\{\boldsymbol{X}_t^{\underline{S},r}:t=0,\ldots,T,r=1,\ldots,R\right\}$, $R\geq 1$, *are Gaussian (condition (GR)), stationary with respect to r (condition (SR)). Assume also that conditions (LR), (F) and (M) are satisfied as well as the conditions*

$$\sup_{t,\underline{s},\underline{S}}\mathrm{E}\left(\left|X_t^{\underline{S}}(\underline{s})\right|^{4+2\delta}\right)<\infty\quad\textit{and}\quad\sum_k\alpha_X(k)^{\delta/(2+\delta)}<\infty$$

for some $\delta > 0$*, and*

$$\sum_{k\in\mathbb{Z}} \left| f^{k}_{\tau_j,\tau_{j'},\underline{u}_j,\underline{u}_{j'}}(\omega_j,\omega_{j'}) \right| < \infty.$$

Then

$$\lim_{R\to\infty} \mathcal{L}\left(\sqrt{R}\left(\tilde{\boldsymbol{f}}^{T,\underline{S},N,R} - \boldsymbol{f}\right)\right) = \mathcal{N}_{2k}\left(0, \boldsymbol{\Sigma}_{2k}\right),$$

where the components of the variance $(2k\times 2k)$*-matrix* $\boldsymbol{\Sigma}_{2k} = \boldsymbol{\Sigma}^{(\omega_{1,1},\omega_{2,1},\ldots,\omega_{1,k},\omega_{2,k})}_{\tau_{1,1},\tau_{2,1},\ldots,\tau_{1,k},\tau_{2,k},\underline{u}_{1,1},\underline{u}_{2,1},\ldots,\underline{u}_{1,k},\underline{u}_{2,k}}$ *can be computed from Lemma 3.1.*

Corollary 3.1. *Under conditions of Theorem 3.2*

$$\sqrt{R}\left(\tilde{\rho}^{T,\underline{S},N,R}_{\tau_1,\tau_2,\underline{u}_1,\underline{u}_2}\left(\omega_1,\omega_2\right) - \rho_{\tau_1,\tau_2,\underline{u}_1,\underline{u}_2}\left(\omega_1,\omega_2\right)\right) \Longrightarrow \mathcal{N}(0,\gamma^2), \tag{13}$$

provided that $f_{\tau_1,\tau_1,\underline{u}_1,\underline{u}_1}\left(\omega_1,\omega_1\right) f_{\tau_2,\tau_2,\underline{u}_2,\underline{u}_2}\left(\omega_2,\omega_2\right) \neq 0$*.*
Here $\gamma^2 = (\nabla^{(\omega_1,\omega_2)}_{\tau_1,\tau_2,\underline{u}_1,\underline{u}_2})\boldsymbol{\Sigma}_6(\nabla^{(\omega_1,\omega_2)}_{\tau_1,\tau_2,\underline{u}_1,\underline{u}_2})'$*, where* ∇ *denotes the gradient operator. The variance* 6×6*-matrix* $\boldsymbol{\Sigma}_6$ *is given in Theorem 3.2, with* $k=3$*,* $\tau_{1,1}=\tau_{2,1}=\tau_{1,3}=\tau_1$*,* $\tau_{1,2}=\tau_{2,2}=\tau_{2,3}=\tau_2$*,* $\underline{u}_{1,1}=\underline{u}_{2,1}=\underline{u}_{1,3}=\underline{u}_1$*,* $\underline{u}_{1,2}=\underline{u}_{2,2}=\underline{u}_{2,3}=\underline{u}_2$*,* $\omega_{1,1}=\omega_{2,1}=\omega_{1,3}=\omega_1$*, and* $\omega_{1,2}=\omega_{2,2}=\omega_{2,3}=\omega_2$*. Moreover,*

$$\begin{aligned}\nabla^{(\omega_1,\omega_2)}_{\tau_1,\tau_2,\underline{u}_1,\underline{u}_2} \;=\; \Bigg(& \frac{-\left|f_{\tau_1,\tau_2,\underline{u}_1,\underline{u}_2}\left(\omega_1,\omega_2\right)\right|^2}{\left(f_{\tau_1,\tau_1,\underline{u}_1,\underline{u}_1}\left(\omega_1,\omega_1\right)\right)^2 f_{\tau_2,\tau_2,\underline{u}_2,\underline{u}_2}\left(\omega_2,\omega_2\right)}\,,\; 0\,,\; \frac{-\left|f_{\tau_1,\tau_2,\underline{u}_1,\underline{u}_2}\left(\omega_1,\omega_2\right)\right|^2}{f_{\tau_1,\tau_1,\underline{u}_1,\underline{u}_1}\left(\omega_1,\omega_1\right)\left(f_{\tau_2,\tau_2,\underline{u}_2,\underline{u}_2}\left(\omega_2,\omega_2\right)\right)^2}\,, \\ & 0\,,\; \frac{2\Re f_{\tau_1,\tau_2,\underline{u}_1,\underline{u}_2}\left(\omega_1,\omega_2\right)}{f_{\tau_1,\tau_1,\underline{u}_1,\underline{u}_1}\left(\omega_1,\omega_1\right) f_{\tau_2,\tau_2,\underline{u}_2,\underline{u}_2}\left(\omega_2,\omega_2\right)}\,,\; \frac{2\Im f_{\tau_1,\tau_2,\underline{u}_1,\underline{u}_2}\left(\omega_1,\omega_2\right)}{f_{\tau_1,\tau_1,\underline{u}_1,\underline{u}_1}\left(\omega_1,\omega_1\right) f_{\tau_2,\tau_2,\underline{u}_2,\underline{u}_2}\left(\omega_2,\omega_2\right)}\Bigg)'.\end{aligned}$$

3.6 Bootstrap approach

Using Corollary 3.1 one may construct confidence interval for spatial time-varying dual-frequency coherence $\rho_{\tau_1,\tau_2,\underline{u}_1,\underline{u}_2}\left(\omega_1,\omega_2\right)$. However, since the asymptotic variance γ^2 depends on unknown parameters, it is in practice very difficult to estimate. Thus, we

present below a bootstrap approach that allows to obtain consistent confidence intervals for $\rho_{\tau_1,\tau_2,\underline{u}_1,\underline{u}_2}(\omega_1,\omega_2)$.

Let us recall that $\left\{X_t^{\underline{S},r}(\underline{s})\right\}$ is stationary in r and nonstationary in t. We will bootstrap our observations in replicates not in time. For that purpose we use the Circular Block Bootstrap (CBB) of Politis and Romano (1992). The CBB is a modification of the Moving Block Bootstrap method (Künsch (1989), Liu and Singh (2018)), which allows to reduce bias of the bootstrap estimator. Below we present how to adapt the CBB algorithm to our problem.

Let us recall that we have R replicates of $\left\{\boldsymbol{X}_t^{\underline{S}}\right\} = \left\{X_t^{\underline{S}}(\underline{s})\right\}$, which we denote by $\boldsymbol{X}^{(r)} = \left\{X_t^{\underline{S},r}(\underline{s})\right\}$, $r = 1,\ldots,R$. Moreover, let B_i, $i = 1,\ldots,R$ be the block of replicates from our sample $\left(\boldsymbol{X}^{(1)},\ldots,\boldsymbol{X}^{(R)}\right)$, that starts with replicate $\boldsymbol{X}^i$ and has the length $b \in \mathbb{N}$, i.e.

$$B_i := \left(\boldsymbol{X}^{(i)},\ldots,\boldsymbol{X}^{(i+b-1)}\right).$$

If $i+b-1 > R$ then the missing part of the block is taken from the beginning of the sample and we get

$$B_i = \left(\boldsymbol{X}^{(i)},\ldots,\boldsymbol{X}^{(R)},\boldsymbol{X}^{(1)},\ldots,\boldsymbol{X}^{(b-R+i-1)}\right)$$

for $i = R-b+2,\ldots,R$.

CBB algorithm

1. Choose a block size $b < R$. Then our sample $\left(\boldsymbol{X}^{(1)},\ldots,\boldsymbol{X}^{(R)}\right)$ can be divided into l blocks of length b and the remaining part is of length r, i.e. $R = lb+r$, $R = 0,\ldots,b-1$.

2. From the set $\{B_1,\ldots,B_R\}$ choose randomly with replacement $l+1$ blocks.

3. Join the selected $l+1$ blocks $(B_1^*, \ldots, B_{l+1}^*)$ and take the first R observations to get the bootstrap sample $\left(\boldsymbol{X}^{*(1)}, \ldots, \boldsymbol{X}^{*(R)}\right)$ of the same length as the original one.

We apply the CBB to get bootstrap estimators of $f_{\tau_1,\tau_2,\underline{u}_1,\underline{u}_2}(\omega_1,\omega_2)$ and $\rho_{\tau_1,\tau_2,\underline{u}_1,\underline{u}_2}(\omega_1,\omega_2)$ and finally to be able to construct confidence intervals for these characteristics. We use the bootstrap algorithm described above. The bootstrap version of $\widetilde{f}^{T,S,N,R}_{\tau_1,\tau_2,\underline{u}_1,\underline{u}_2}(\omega_1,\omega_2)$ is of the form

$$\tilde{f}^{*,R}_{1,2}(\omega_1,\omega_2) = \tilde{f}^{*,T,\underline{S},N,R}_{\tau_1,\tau_2,\underline{u}_1,\underline{u}_2}(\omega_1,\omega_2) = \frac{1}{R}\sum_{r=1}^{R}\tilde{I}^{*,r}_{1,2}(\omega_1,\omega_2) \tag{14}$$

$$= \frac{1}{4\pi^2 R}\sum_{r=1}^{R}\tilde{d}^{*,r}_1(\omega_1)\,\overline{\tilde{d}^{*,r}_2(\omega_2)}, \tag{15}$$

where for $i=1,2$,

$$\begin{aligned}\widetilde{d}^{*,r}_i(\omega) &= \widetilde{d}^{*,T,\underline{S},N,r}_{\tau_i,\underline{u}_i}(\omega) := \sum_{t_i}\sum_{\underline{s}_i} W_{\tau_i}(t_i) w_{\underline{u}_i}(\underline{s}_i) d^{*,T,\underline{S},r}_{t_i,\underline{s}_i}(\omega) \\ &= \sum_{t_i}\sum_{\underline{s}_i} W_{\tau_i}(t_i) w_{\underline{u}_i}(\underline{s}_i) \sum_{k_i=t_i-N}^{t_i+N-1} X^{*,T,\underline{S},r}_{k_i}(\underline{s}_i)\, e^{-i\omega k_i}.\end{aligned}$$

3.6.1 Bootstrap consistency

Below we state the consistency of our bootstrap approach for the spatial time-varying dual-frequency coherence function. The bootstrap estimator of the spatial coherence is defined as

$$\tilde{\rho}^{*,T,\underline{S},N,R}_{\tau_1,\tau_2,\underline{u}_1,\underline{u}_2}(\omega_1,\omega_2) := \frac{\left|\tilde{f}^{*,T,\underline{S},N,R}_{\tau_1,\tau_2,\underline{u}_1,\underline{u}_2}(\omega_1,\omega_2)\right|^2}{\tilde{f}^{*,T,\underline{S},N,R}_{\tau_1,\tau_1,\underline{u}_1,\underline{u}_1}(\omega_1,\omega_1)\,\tilde{f}^{*,T,\underline{S},N,R}_{\tau_2,\tau_2,\underline{u}_2,\underline{u}_2}(\omega_2,\omega_2)}.$$

Theorem 3.3. *Under conditions of Theorem 3.2 and assuming that* $b^{-1} + R^{-1}b = o(1)$ *the CBB is consistent i.e.,*

$$\sup_{x\in\mathbb{R}}\left|P^*\left(\sqrt{R}\left(\tilde{\rho}^{*,T,\underline{S},N,R}_{\tau_1,\tau_2,\underline{u}_1,\underline{u}_2}(\omega_1,\omega_2) - \frac{\left(\mathrm{E}^*\Re\left(\tilde{f}^{*,T,\underline{S},N,R}_{\tau_1,\tau_2,\underline{u}_1,\underline{u}_2}(\omega_1,\omega_2)\right)\right)^2 + \left(\mathrm{E}^*\Im\left(\tilde{f}^{*,T,\underline{S},N,R}_{\tau_1,\tau_2,\underline{u}_1,\underline{u}_2}(\omega_1,\omega_2)\right)\right)^2}{\mathrm{E}^*\left(\tilde{f}^{*,T,\underline{S},N,R}_{\tau_1,\tau_1,\underline{u}_1,\underline{u}_1}(\omega_1,\omega_1)\right)\mathrm{E}^*\left(\tilde{f}^{*,T,\underline{S},N,R}_{\tau_2,\tau_2,\underline{u}_2,\underline{u}_2}(\omega_2,\omega_2)\right)}\right) \le x\right)\right.$$
$$\left. - P\left(\sqrt{R}\left(\tilde{\rho}^{T,\underline{S},N,R}_{\tau_1,\tau_2,\underline{u}_1,\underline{u}_2}(\omega_1,\omega_2) - \rho_{\tau_1,\tau_2,\underline{u}_1,\underline{u}_2}(\omega_1,\omega_2) \le x\right)\right)\right| \xrightarrow{p} 0 \quad as \quad R\longrightarrow\infty.$$

While applying block bootstrap a natural question that appears concerns the choice of the block length. In the case of stationary sequences this problem is well investigated (see Lahiri (2003)). It is well known that for the CBB the optimal block length obtained by minimization of the mean squared error of the bootstrap estimator is $b = \mathcal{O}(R^{1/3})$ (see Theorem 5.4 in Lahiri (2003)).

4 Real Data Analysis

In order to illustrate the previously developed methodology, we apply it to a real data set that has been collected in order to assess the VWM performance of subjects. We will use our method to potentially identify specific patterns in the dynamic functional connectivity related to the capacity of the VWM.

4.1 Experiment and data analysis pipeline

The experiment consists in the following three steps (an illustration is provided in Section 2 of the Companion document):

- memory set: a patient is placed in front of a computer screen. An arrow appears and the patient has 2 seconds to memorize its orientation and color,

- retention time: then a blank screen appears for 0.3 seconds, for the next 0.1 second many arrows appear to knock out the immediate memory, then a blank screen appears again for 0.9 second,
- memory test: finally, the patient, using a joystick, has to reproduce the orientation and the color of the arrow. This final step lasts 1.7 seconds.

Notice that the RGB color scale is presented to the patient on a circle. Henceforth we compute the VWM error for both orientation and color as an angle between the true one and the patient guess. The set of bivariate measures of the errors is denoted hereafter as $\{\mathbf{y}^{(r)} \in (0, 2\pi]^2, r = 1, \ldots, R\}$.

While the patient is performing these tasks the EEG traces are recorded. We use a standard Hydrocel geodesic sensor with 128 electrodes that are placed on the scalp of a patient at specific spatial locations. These electrodes record the electric potential (in micro-volts) over the time at a sampling rate of 256 Hz. The test is replicated 2400 times.

Once the data are collected, we apply the standard preprocessing pipeline (see Bigdely-Shamlo et al. (2015)) to remove eye blink and eye movement, for filtering... Notice that the Hydrocel localization has been converted to the 10-10 standard to be used with the R package *EEGkit* (Helwig, 2018).

Hereafter, we denote the set of replicated spatially localized EEG traces as $\{\boldsymbol{X}_t^{\underline{S},r}(\underline{s}), \underline{s} \in \mathcal{M}, r = 1, \ldots, R\}$, where $\mathcal{M}$ is the set of the projected coordinates of the electrodes on the two-dimensional plane.

In the sequel, we consider the two following frequency bands α and β ($[7.5, 12.5]$-Hz and $[12.5, 20]$-Hz., respectively), denoted as Ω_α and Ω_β.

Following the description of our method and its theoretical performances, it is clear that the estimation of the spatial time-varying dual-frequency Loève spectrum relies on pooling

information from many replicated time series. Hence, in order to identify specific patterns in the STVDF Loève spectrum accordingly to the VWM performance we propose the following data analysis pipeline:

- perform unsupervised clustering of the EEG traces accordingly to the response variables,
- within each cluster of the corresponding EEG traces, we perform the estimation of the spatial time-varying dual-frequency coherence function.

4.2 Clustering with toroidal mixture

The Figure 2 represents the bivariate errors response for all replicates available for our test subject. For practical purposes the distribution of the errors is centered around (π, π) rather than $(0, 0)$. We observe seemingly more precise quality of memorization for color than for angles. We fit an L components mixture of bivariate wrapped normal distributions using the "BAMBI" R package(Chakraborty and Wong, 2019, 2018). The mixture density is given by:

$$f(\mathbf{y}|p_1, \ldots, p_{L-1}; \theta_1, \ldots, \theta_L) = \sum_{l=1}^{L} p_l f_{WN}(y|\theta_l)$$

$$f_{WN}(\mathbf{y}|\theta_l) = f_{WN}(.|\mu_l, \Sigma_l) = \frac{\sqrt{\kappa_1\kappa_2 - \kappa_3}}{2\pi} \sum_{(\omega_1,\omega_2)\in\mathbb{Z}^2} \exp\left\{-\frac{1}{2}\left\{\kappa_{1,l}(y_1 - \mu_{1,l} - 2\pi w_1)^2\right.\right.$$

$$\left.\left.+\kappa_{2,l}(y_2 - \mu_{2,l} - 2\pi\omega_2)^2 + 2\kappa_{3,l}(y_1 - \mu_{1,l} - 2\pi w_1)(y_2 - \mu_{2,l} - 2\pi\omega_2)\right\}\right\},$$

where L is an unknown number of components, p_l are such that $\sum_{l=1}^{L} p_l = 1$, $y_1, y_2, \mu_{1,l}, \mu_{2,l} \in [0, 2\pi)$, $\kappa_{1,l}, \kappa_{2,l} > 0$, $\kappa_{3,l}^2 \leq \kappa_{1,l}\kappa_{2,l}$ and

$$\Delta_l = \begin{pmatrix} \kappa_{1,l} & \kappa_{3,l} \\ \kappa_{3,l} & \kappa_{2,l} \end{pmatrix}.$$

We found out that a mixture model with $L = 2$ components gives a satisfying classification as testified on the Figure 2. Table (1) summarizes the parameter estimates. The first component (colored in red) represents 'poor' memorization capacity and concerns about 10 percent of the available replicates. The second component (colored in green) is nicely centered around π showing that on the average the memorization is unbiased for both colors and angles. The precision parameters κ's show much lower precision for orientation errors. This is probably due to the additional mass observed around 0 and 2π which presumably corresponds to guessed values for which the patient recalled well the direction but inverted the orientation. An interesting follow up study could focus on studying clusters of replicates accordingly to the orientation inversion or not. Nevertheless, only a few replicates are concerned so that the estimation of the coherence function cannot be precisely done with this dataset.

Parameters	Component 1	Component 2
p	0.093 (0.082, 0.11)	0.91 (0.89, 0.92)
κ_1	0.31 (0.097, 0.61)	2.60 (2.60, 2.60)
κ_2	0.00029 (1e-04, 7e-04)	16.75 (16.75, 16.75)
κ_3	-1.73 (-1.95, -1.58)	2e-04 (2e-04, 2e-04)
μ_1	4.91 (4.64, 5.11)	3.14 (3.14, 3.14)
μ_2	4.64 (4.53, 4.77)	3.16 (3.16, 3.16)

Figure 1: Parameters of the mixture of bivariate wrapped-normal distributions

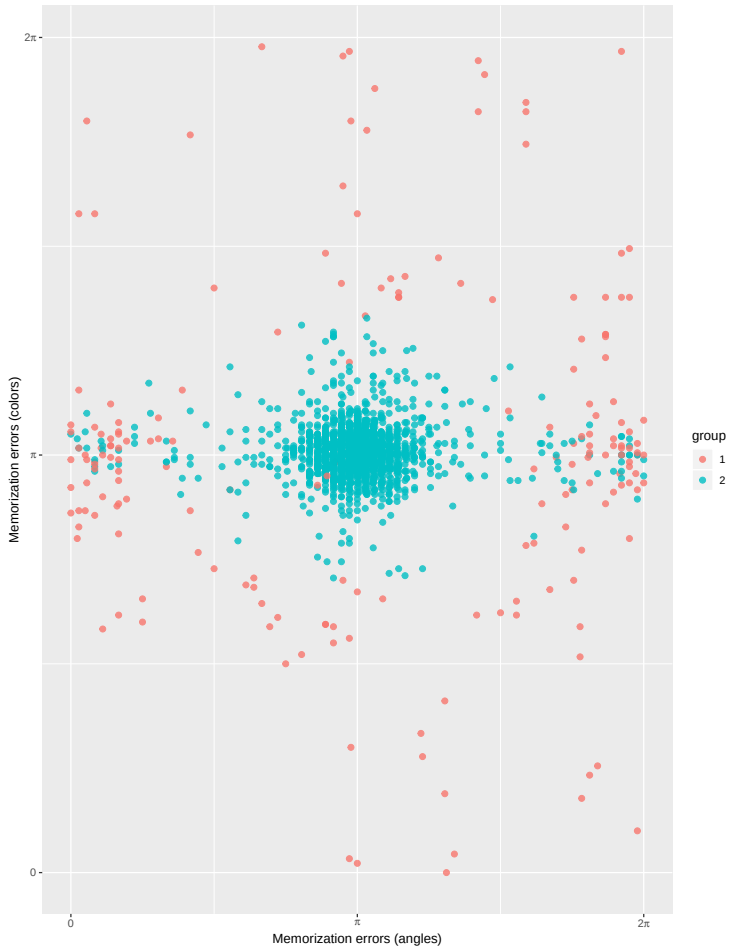

Figure 2: Angular errors associated to each replicates; x-axis: arrow orientation error; y-axis: arrow color error. The elements part of the first and second component mixture are in red and blue.

4.3 Two-stages procedure for label-specific estimation of the spatial time-varying dual-frequency coherence

In our approach we are dealing with a eight dimensional coherence function and our methodology involves bootstrapping over the replicated time-spatial random arrays. This seems obviously to be a computationally cumbersome approach. Nevertheless, the specific characteristics of our data analysis reduces significantly the computational demand. First, we estimate a coherence, which is basically a correlation coefficient, therefore we are only interested in "large" values. Second, in EEG data analysis we are interested in estimating the coherence between a few frequency bands that are of interest. Moreover, from a neurophysiological stand point it is reasonable to assume that the brain connectivity is sparse at each time of observation. Third, the spatial smoothing ensure pooling information across space but ultimately we are only interested in initial locations sampling of our EEG electrodes. Finally, we will not evaluate the coherence across two different time points τ_1, τ_2. These facts suggest to design a two-stage method as described below and which makes our methodology computationally feasible:

- compute the spatial time-varying dual-frequency coherence $\widetilde{\rho}^{T,\underline{S},N,R}_{\tau,\tau,\underline{u}_1,\underline{u}_2}(\Omega_1, \Omega_2)$,
- apply the bootstrap method only for spatial and time points of interest, i.e., when the estimate $\widetilde{\rho}^{T,\underline{S},N,R}_{\tau,\underline{u}_1,\underline{u}_2}(\Omega_1, \Omega_2)$ is above a user-specific threshold value.

Our final step is to built connectivity matrices which relate different spatial locations at a time point and for a given combination of frequency bands. From these matrices we construct sequence of graphs as one of displayed in the Figure 3. The lines are drawn in between locations for which the lower limit of the left-sided bootstrap confidence interval for

the dual-frequency coherence passes over a predefinite threshold value of 0.3. The graphs represent the connectivity estimated from the set of replicates related to poor (left-hand side) and to good (right-hand side) VWM capacity. A sequence of these graphs at different time points is presented in the Section 4 of the companion document. It allows us to capture the dynamics of the (dual-frequency)-dependent functional connectivity.

More specifically, we observe that the persistence of connections in the first stage of the experiment, corresponding to 'memory set', between the $\alpha - \beta$ frequency bands in the prefrontal cortex (channels: FP1, FPZ, FP2), lasts on much longer period for the group 2 than for the group 1. That is when the replicate results in lower VWM errors. Our results are consistent with other known results that highlight the role of the prefrontal cortex for encoding task relevant information in working memory tasks (Lara and Wallis (2015); Funahasi (2017)). Our results additionally suggest that the functional connectivity occurs at different oscillating frequencies.

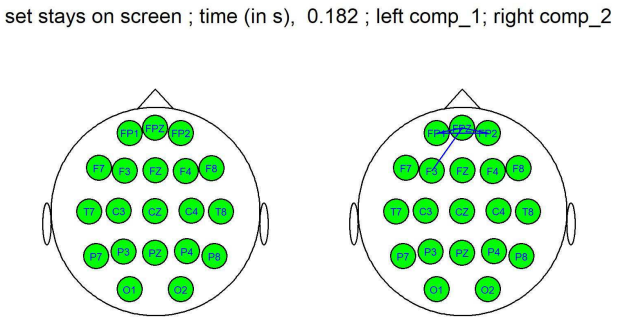

Figure 3: Estimated functional connections between α and β frequency bands associated to poor VWM results (left-side graph), to good VWM results (right-side graph).

Remark 4.1. *In our analysis we choose the block length in the CBB step to be* $b = \sqrt[3]{R}$. *The size of the Fourier window along the time is chosen in an ad hoc way to ensure the estimability of the frequency bands of interest and to preserve a reasonable time resolution.*

5 Conclusions

We proposed a method for dual-frequency coherence estimation based on replicated, spatially localized time-varying harmonizable time series. We showed the ability of this method to describe the dynamic functional connectivity across different frequencies of EEG time series. Our study reveals different alpha-beta connectivity patterns in the prefrontal cortex

during the memorization stage of the experiment that may be related to the capacity of the visual working memory.

SUPPLEMENTARY MATERIAL

Companion Document: Contains some connectivity graphs and all proofs of the paper. For pedagogical purposes we provided all detailed proofs in the particular case of location dependent Loève spectrum estimation. (pdf file)

References

Barton, B. and A. Brewer (2013). Visual working memory in human cortex. *Psychology (Irvine) 4(8)*, 655–662.

Bigdely-Shamlo, N., T. Mullen, C. Kothe, K.-M. Su, and K. A. Robbins (2015). The prep pipeline: standardized preprocessing for large-scale eeg analysis. *Frontiers in Neuroinformatics 9*, 16.

Brockwell, P. and R. Davis (1991). In *Time Series: Theory and Methods*. Springer Verlag, New York.

Chakraborty, S. and S. W. Wong (2019). *BAMBI: Bivariate Angular Mixture Models*. R package version 2.1.0.

Chakraborty, S. and S. W. K. Wong (2018). Bambi: An r package for fitting bivariate angular mixture models. Technical report.

Cramér, H. (1961). On some classes of nonstationary stochastic processes. *Proc. Fourth Berkeley Symp. Math. Stat. and prob., University California Berkeley 2*, 55–77.

Dahlhaus, R. *Chapter 13: Locally Stationary Processes*, Volume 30.

Dai, Z., J. de Souza, J. Lim, P. M. Ho, Y. Chen, J. Li, N. Thakor, A. Bezerianos, and Y. Sun (2017). Eeg cortical connectivity analysis of working memory reveals topological reorganization in theta and alpha bands. *Frontiers in Human Neuroscience 11*, 237.

Doukhan, P. (1994). In *Mixing: properties and examples*. Springer series in statistics.

Fougnie, D., J. Suchow, and G. Alvarez (2012). Variability in the quality of visual working memory. *Nature communications*.

Funahasi, S. (2017). Working memory in the prefrontal cortex. *Brain sciences 7(49)*.

Gündoğdu, U. and A. Akan (2010). Eeg analysis using bi-frequency coherence. In *2010 18th European Signal Processing Conference*, pp. 944–948.

Gorrostieta, C., H. Ombao, R. Prado, S. Patel, and E. Eskandar (2012). Exploring dependence between brain signals in a monkey during learning. *Journal of time series analysis 33(5)*, 771–778.

Gorrostieta, C., H. Ombao, and R. von Sachs (2019). Time-dependent dual-frequency coherence in multivariate non-stationary time series. *Journal of Time Series Analysis 40*(1), 3–22.

Grimault, S., N. Robitaille, C. Grova, J. Lina, A. Dubarry, and P. Jolicoeur (2009). Oscillatory activity in parietal and dorsolateral prefrontal cortex during rentention in visual

short-term memory: additive effects of spatial attention and memory load. *Human Brain Mapping 30*, 3378–3392.

Helwig, N. E. (2018). *eegkit: Toolkit for Electroencephalography Data*. R package version 1.0-4.

Hurd, H. and A. Miamee (2007). In *Periodically Correlated Random Sequences: Spectral Theory and Practice*. Wiley Series in Probability and Statistics.

Künsch, H. (1989). The jackknife and the bootstrap for general stationary observations. *Ann. Statist. 17*, 1217–1241.

Lahiri, S. (2003). In *Resampling Methods for Dependent Data*. Springer, New York.

Lara, H. and J. Wallis (2015). The role of the prefrontal cortex in working memory: a mini review. *Frontiers in neuroscience 9*.

Li, L., J.-W. Zhang, and T. Jiang (2011). Visual working memory load-related changes in neural activity and functional connectivity. *PLOS one 6(7)*, 1–14.

Liu, R. and K. Singh (2018). In N. Y. Wiley Ser. Probab. Math. Statist. Probab. Math. Statist. Wiley (Ed.), *Moving block jackknife and bootstrap capture weak dependence*.

Loève, M. (1948). Fonctions aléatoire du second ordre. In Gauthier-Villars (Ed.), *P. Levy's Processus stochastiques et mouvement Brownien*, pp. 228–252. Paris.

Luck, S. and E. Vogel (2013). Visual working memory capactiy: from psychophysics and neurobiology to individual differences. *Trends Cogn. Sci. 17(8)*, 391–400.

Ombao, H., X. Shao, E. Rykhlevskaia, M. Fabiani, and G. Gratton (2008). Spatio-spectral analysis of brain signals. *Statistica Sinica 18*, 1465–1482.

Pascual-Marqui, R., P. Faber, T. Kinoshita, Y. Kitaura, K. Kochi, P. Milz, K. Nishida, and M. Yoshimura (2016). The dual frequency rv-coupling coefficient: a novel measure for quantifying cross-frequency information transactions in the brain. *arXiv:1603.05343*.

Politis, D. and J. Romano (1992). *A circular block-resampling procedure for stationary data.*

Rozanov, Y. (1959). Spectral analysis of abstract function. *Th. Prob. Appl. 4*, 271–287.

Sauseng, P., W. Klimesch, M. Schabus, and D. M. (2005). Fronto-parietal eeg coherence in theta and upper alpha reflect central executive functions of working memory. *Int J Psychophysiol 57(2)*, 97–103.

Soedjak, H. *Chapter 7: Bispectral density estimation in harmonizable processes.*